Published in final edited form as:
J Am Chem Soc. 2012 October 24; 134(42): 17338–17341. doi:10.1021/ja3063698.

Amino Naphthalenyl-2-Cyano-Acrylate (ANCA) Probes Fluorescently Discriminate between Amyloid-βand Prion Plaques in Brain

Kevin Cao[†], **Mona Farahi**[‡], **Marianna Dakanali**[†], **Willy M. Chang**[†], **Christina J. Sigurdson**[‡], **Emmanuel A. Theodorakis**[†,*], and **Jerry Yang**[†,*]

[†]Department of Chemistry and Biochemistry, University of California, San Diego, La Jolla, California 92093-0358, United States

[‡]Department of Pathology, University of California, San Diego, La Jolla, California 92093-0612, United States

Abstract

A major challenge for diagnosing and monitoring the progression of amyloid-based diseases is the capability to distinguish between amyloid deposits that are associated with related, but distinctly different, diseases. Here, we demonstrate that Amino Naphthalenyl-2-Cyano-Acrylate (ANCA)-based probes can fluorescently discriminate between different types of amyloid deposits in brain. This discriminating behavior is due to the stabilization of the ground versus excited states of these probes as a function of the polarity of their microenvironment (i.e. within the binding pocket on the amyloid). This property makes it possible for the first time to estimate the inherent static relative permittivity of the binding pocket of each amyloid within tissue. The capability to selectively follow the deposition of specific amyloids in tissue may provide important information for therapeutic development that is not readily accessible from currently available technology.

Amyloid plaque accumulation in the brain is the hallmark of many neurodegenerative disorders, including Alzheimer's (AD) and Creutzfeldt-Jakob (CJD) disease.[1,2] Approaches to clinically diagnose and monitor the progression of these diseases include targeting of amyloid deposits with small molecule imaging agents.[3-5] Along these lines, an amyloid-labeling probe for use in positron emission tomography (PET) has recently been shown to be a clinically useful diagnostic agent for AD.[6,7] While PET imaging represents a great first step toward the diagnosis of neurodegenerative diseases, this technique is limited by the binary nature of the radioactive signal that does not allow for discrimination between amyloids associated with different, but closely related, diseases. Alternative techniques that can discern between different types of amyloids may offer important information necessary to develop effective treatment strategies that are tailored to specific diseases.

Fluorescence-based imaging of amyloids has emerged as a potentially lower cost, more accessible, and nonradioactive alternative method to PET.[8-16] In principle, fluorescence-based-probes offer an advantage over their radio-active counterparts since their fluorescence profile could be used to distinguish different amyloids in tissue. Here, we report the ability of Amino Naphthalenyl-2-Cyano-Acrylate (ANCA)-based probes (for a generic structure see Table 1) to fluorescently discriminate between deposits in brain derived from amyloid-β

[*]Corresponding Author jerryyang@ucsd.edu or etheodor@ucsd.edu.

ASSOCIATED CONTENT Details for the synthesis of compounds **1-3**, experimental protocols for the staining of plaques in neuronal tissue, and for binding and fluorescence studies. This information is available free of charge via the Internet at http://pubs.acs.org.

(Aβ) peptides associated with AD or from prion (PrP^{Sc}) proteins associated with prion disease (Figure 1).

We previously reported that ANCA probes (**1-3**, Table 1) could label Aβ plaques in human brain tissue sections from AD patients.[15] Brain sections stained with these probes showed good overlap of fluorescence with a mouse monoclonal anti-human Aβ IgG, demonstrating that these probes could mark the location of Aβ deposits with good specificity compared to surrounding background tissue. The ANCA probes fluoresce by a photon-induced dipole mechanism,[14,17] where the electron rich amine functionality, attached to the naphthalene moiety, can donate electron density to the electron deficient cyano ester through the π-system of the ANCA scaffold (Table 1)-[15,18] The emission of these compounds is enhanced upon restriction of the rotation around the single bonds between the donor (amine) and acceptor (cyano ester) groups. The ANCA probes, therefore, exhibit a large enhancement in fluorescence properties upon binding to amyloid substrates compared to the weaker fluorescence of the free compounds when in solution (see Figure S1 in the SI).

To explore the ability of the ANCA probes to fluorescently label amyloid deposits from proteins other than Aβ in tissue, we compared fluorescence micrograph images of plaques derived from Aβ (Figure 1A) and PrP^{Sc} (Figure 1B) stained with **1** in frozen brain sections (i.e., unfixed) from mouse models for AD and prion disease.[19-21] Importantly, **1** exhibited excellent capability to label amyloid plaques in both tissues and displayed a visually observable difference in the color emitted upon staining of the plaques. Probes **2** and **3** exhibit similar properties (see Figure S3 in SI).

Table 1 displays that the ANCA probes bound to amyloid deposits exhibit a difference in maximal emission wavelength (λ_{max}) of ~20 nm, depending on the type of amyloid protein present in the plaque. Remarkably, the variability the observed λ_{max} between plaques was quite narrow (± 2-3 nm from inspection of ≥ 25 plaques in each sample). Moreover, Aβ plaques stained with **1** from different parts of the brain (e.g., hippocampus, hypothalamus, cortex) from the same mouse all exhibited essentially the same emission λ_{max} (± 3 nm). Additionally, prion plaques stained with **1** from the corpus callosum of different mice also exhibited essentially the same emission λ_{max} (± 2 nm). In contrast, we did not observe such fluorescence discrimination upon staining of the plaques with Congo red (see Figure S4 in the SI). These surprising results prompted us to investigate the origin of fluorescence discrimination by **1-3**.

Previous studies in solution have shown that the small differences in the environment of proteins[22-26] and lipids[27] can affect the Stokes shift of bound fluorophores.[28] If the time dependence of fluorescence polarization of probes **1-3** can be neglected—that is, if we assume that any reorientation molecules within the binding pocket of the amyloid proteins is fast compared to the lifetime of the excited state of the probes—the dependence of the polar environment on the frequency of the absorbance and fluorescence emission spectra of **1-3** can be approximated by the Ooshika-Lippert. Mataga (OLM) equation:[27,29,30]

$$\Delta v = \frac{2\left(\mu_e - \mu_g\right)^2}{ha^3}\left(\frac{\varepsilon_0 - 1}{2\varepsilon_0 + 1} - \frac{n^2 - 1}{2n^2 + 1}\right) \quad (1)$$

where Δv is the average frequency of the Stokes shift,[31] μ_e and μ_g are the dipole moments of the molecules in the excited state and ground state respectively, h is Plank's constant, a is the approximate radius of the molecules assuming a spherical cavity with a rigid dipole at the center, ε_0 is the static relative permittivity (i.e., dielectric constant) of the dielectric continuum surrounding the molecules, and n is the refractive index of the medium.

Since the frequency of absorption for molecules **1-3** remains relatively constant when measured in different solvents of various polarities, we found an approximately linear relationship between the Stokes shifts of **1-3** and their observed λ_{max} for fluorescence emission (see Figure S5 in the SI). This linear correlation allows us to use only the λ_{max} of emission to analyze the effect of the polar environment within the binding pockets of the amyloids on the fluorescence properties of **1-3**.[32] Equation 1 could, therefore, be simplified to:[27]

$$\frac{1}{\lambda_{max}\,(\text{Emission})} = C_1\left(\frac{\varepsilon_0 - 1}{2\varepsilon_0 + 1} - \frac{n^2 - 1}{2n^2 + 1}\right) + C_2 \quad (2)$$

where C_1 and C_2 are constants that reflects several inherent properties of the ANCA probes.

Figure 2A-C (open circles, ○) plots the dependence of $1/\lambda_{max}$ for fluorescence emission of **1-3** in solvents of various polarities (see Figure S6 in the SI) as a function of the static relative permittivity (ε_0) and refractive index (n) of each sol-vent according to eq. 2. The observed linear behavior shown in Figures 2A-C suggests that the OLM equation (eq. 1) describes fairly well the dependence of the observed fluorescence of compounds **1-3** on the polarity of their surrounding environment. These results suggest that the origin of the observed fluorescence discrimination between the two different types of amyloid deposits using probes **1-3** could indeed be simply explained by small differences in the polar environment within the binding pockets of the amyloid proteins.

In order to gain some additional insight into the nature of the polar environment within the binding pockets of the amyloid tissues, we replotted the dependence of $1/\lambda_{max}$ for fluorescence emission of **1-3** in different solvents as a function of ε_0 only, while ignoring the refractive index of the solvent (Figure 2A-C, open squares,).[27] We found that the linear fit of $1/\lambda_{max}$ versus $(\varepsilon_0\text{-}1)/(2\varepsilon_0\text{+}1)$ was consistently better compared to when the refractive index was included as in eq. 2 (see Figure S7 in the SI). This suggests that the static relative permittivity (ε_0) dominated the dependence of the polar environment on the λ_{max} for fluorescence emission of **1-3**.[33] This simple relationship between λ_{max} and ε_0, hence, made it possible to estimate the static relative permittivity of the binding pockets of the two different amyloids in tissue by the observed emission maxima of plaques stained with **1-3** (Figure 2D). Satisfyingly, the estimated ε_0 values for the two amyloids were in fairly good agreement (given the assumptions and approximations made in equations 1 and 2), regardless of which ANCA probe was used for measurement. The data reveals that both amyloid binding pockets are relatively hydrophobic as expected, but that the permittivity within the binding pocket of prion plaques is roughly two-fold greater than the permittivity within the binding pocket of Aβ plaques. To provide a reference point for calibration, we estimate the dielectric constants of the binding pocket of Aβ and prion plaques to be roughly similar to diethyl ether (ε_0 =4.27) and tetrahydrofuran (ε_0 = 7.52), respectively.[34]

Although small differences in the polar environment within the binding pockets of the amyloids can reasonably account for the observed fluorescence discrimination of the amyloids with probes **1-3**, we tested another plausible explanation for this observation. We considered that acid-base interactions between the amyloid and the probes could affect the electron donor capability of the amine group of these probes, thus affecting their observed emission profiles. To investigate this possibility, we examined the excitation and emission profiles of **1-3** as a function of pH in free aqueous solution (Figure 3).

Figure 3A,C shows that probes **1** and **2** exhibit a sharp 100-125 nm change in excitation maxima at a pH of ~4.2 and ~1.7, respectively. These changes presumably reflect the

protonation of the nitrogen donor of the piperidine in **1** or morpholine in **2**, and provide an estimate of the pKa's of the protonated forms of these groups. A much smaller change in excitation λ_{max} (~ 10 nm) was observed for **3** at a pH of ~6.9, which presumably reflects the pKa of the protonated N-methyl tertiary amine. More importantly, the emission profiles of **1**-**3** (Figures 3B, D, and F) in acidic (pH 3.8) versus neutral (pH 7.8) solutions indicate that only probe **1** should exhibit a strong (~125 nm) difference in emission λ_{max} when bound to amyloid plaques, if the origin of fluorescence discrimination was due to an acid-base interaction.[35] Since we observe a difference (~20 nm) in emission λ_{max} between Aβ versus prion plaques upon staining with all three probes **1**-**3**, it is unlikely that the origin of fluorescence discrimination is due to acid-base interactions between the probes and the proteins within the binding pocket of the amyloid deposits.

In conclusion, we present a set of fluorescent amyloid-binding probes that can report a different color of fluorescence emission when bound to different types of amyloid deposits in tissue samples. The origin of this fluorescence discrimination most likely arises from the sensitivity of these probes to the polar environment within the binding pocket of an amyloid plaque. Subtle changes to the structure (i.e., electron donor moiety) in these ANCA probes make it possible to tune the spectral window of fluorescence discrimination. The strong correlation between fluorescence emission of the probes and polarity of the environment afforded estimates of the static relative permittivity of the binding pocket in the amyloid plaques. Analysis of amyloid deposits in tissue revealed that the prion deposits exposed a significantly more polar environment to the probes than the Aβ deposits. This previously unreported, fundamental difference between these two types of amyloids make it possible to distinguish them in tissue by simple inspection of the fluorescence emission of molecules that target them. Given the recent findings that amyloiddeposition in the brain of AD patients may be paralleled by deposition of amyloids in the retinal tissue[36-41] or lens[42,43] of the eye, optical inspection of amyloid deposits in the eye may represent an exciting opportunity for diagnosing and monitoring the progression of amyloid-associated diseases. Fluorescent amyloid imaging agents such as the ANCA compounds may, therefore, have practical ophthalmic applications in living patients to help distinguish between closely-related diseases where the symptoms and pathological characteristics show many similarities.[44,45] Efforts to examine the scope of these probes for discriminating amyloid deposits associated with diseases other than Alzheimer's and prion diseases are currently underway.

Supplementary Material

Refer to Web version on PubMed Central for supplementary material.

Acknowledgments

Financial support from the NIH [CA 133002 (EAT) and R01NS069566 (CS)] is gratefully acknowledged. We also thank the NSF for financial support [CHE-9709183, CHE-0741968, and CHE-0847530 (JY)]. We thank Dr. Christina C. Capule for her help with the binding studies. We also thank Dr. Edward Koo for the brain samples from AD transgenic mice.

REFERENCES

(1). Ross CA, Poirier MA. Nature Med. 2004:S10–S17. [PubMed: 15272267]

(2). Irvine GB, El-Agnaf OM, Shankar GM, Walsh DM. Mol. Med. 2008; 14:451–464. [PubMed: 18368143]

(3). Nordberg A. Curr. Opin. Neurol. 2007; 20:398–402. [PubMed: 17620873]

(4). Ono M, Saji H. Int. J. Mole. Imag. 2011:543267.

(5). Xiong K-L, Yang Q-W, Gong S-G, Zhang W-G. Nucl. Med. Commun. 2010; 31:4–11. [PubMed: 19972633]

(6). Clark CM, Schneider JA, Bedell BJ, Beach TG, Bilker WB, Mintun MA, Pontecorvo MJ, Hefti F, Carpenter AP, Flitter ML, Krautkramer MJ, Kung HF, Coleman RE, Doraiswamy PM, Fleisher AS, Sabbagh MN, Sadowsky CH, Reiman EP, Zehntner SP, Skovronsky DM. J. Am. Med. Assoc. 2011; 305:275–283.

(7). Camus V, Payoux P, Barre L, Desgranges B, Voisin T, Tauber C, Joie R, Tafani M, Hommet C, Chetelat G, Mondon K, Sayette V, Cottier JP, Beaufils E, Ribeiro MJ, Gissot V, Vierron E, Vercouillie J, Vellas B, Eustache F, Guilloteau D. Eur. J. Nucl. Med. Mol. Imaging. 2012; 39:621–631. [PubMed: 22252372]

(8). Hintersteiner M, Enz A, Frey P, Jaton A-L, Kinzy W, Kneuer R, Neumann U, Rudin M, Staufenbiel M, Stoeckli M, Wiederhold K-H, Gremlich H-U. Nat. Biotech. 2005; 23:577–583.

(9). Nesterov EE, Skoch J, Hyman BT, Klunk WE, Bacskai BJ, Swager TM. Angew. Chem. Int. Ed. 2005; 44:5452–5456.

(10). Raymond SB, Skoch J, Hills ID, Nesterov EE, Swager TM, Bacskai BJ. Eur. J. Nucl. Med. Mol. Imaging. 2008; 35:S93–S98. [PubMed: 18236039]

(11). Li Q, Lee JS, Ha C, Chan BP, Yang G, Wen BG, Chang YT. Angew. Chem. Int. Ed. 2004; 43:6331–6335.

(12). Ran C, Xu X, Raymond SB, Ferrara BJ, Neal K, Bacskai BJ, Medarova Z, Moore A. J. Am. Chem. Soc. 2009; 131:15257–15261. [PubMed: 19807070]

(13). Ono M, Ishikawa M, Kimura H, Hayashi S, Matsumura K, Watanabe H, Shimizu Y, Cheng Y, Cui M, Kawashima H, Saji H. Bioorg. Med Chem. 2010; 20:3885–3888.

(14). Sutharsan J, Lichlyter D, Wright NE, Dakanali M, Haidekker MA, Theodorakis EA. Tetrahedron. 2010; 66:2582–2588. [PubMed: 20694175]

(15). Chang WM, Dakanali M, Capule CC, Sigurdson CJ, Yang J, Theodorakis EA. ACS Chem. Neurosci. 2011; 2:249–255. [PubMed: 21743829]

(16). Aslund A, Sigurdson CJ, Klingstedt T, Grathwohl S, Bolmont T, Dickstein DL, Glimsdal E, Prokop S, Lindgren M, Konradsson P, Holtzman DM, Hof PR, Heppner FL, Gandy S, Jucker M, Aguzzi A, Hammarstrom P, Nilsson KPR. ACS Chem. Biol. 2009; 4:673–684. [PubMed: 19624097]

(17). Haidekker MA, Theodorakis EA. Org. Biomol. Chem. 2007; 5:1669–1678. [PubMed: 17520133]

(18). Sutharsan J, Dakanali M, Capule CC, Haidekker MA, Yang J, Theodorakis EA. ChemMedChem. 2010; 5:56–60. [PubMed: 20024978]

(19). Sigurdson CJ, Aguzzi A. Biochim. Biophys. Acta. 2007; 1772:610–618. [PubMed: 17223321]

(20). Williams ES. Vet. Pathol. 2005; 42:530–549. [PubMed: 16145200]

(21). Here, we used tissues derived from mice since human tissues containing prion deposits poses significant safety concerns and is not readily available. In the case of Aβ deposits, we chose to use brain sections from mice in order to maintain the same organism for comparison with brain sections containing prion deposits.

(22). Mishra R, Sjölander D, Hammarström P. Mol. BioSyst. 2011; 7:1232–1240. [PubMed: 21279219]

(23). Brandenburg E, v Berlepsch H, Koksch B. Mol. BioSyst. 2012; 8:557–564. [PubMed: 22116468]

(24). Benzeid H, Mothes E, Essassi EM, Faller P, Pratviel GCR. Chimie. 2012; 15:79–85.

(25). Nilsson KPR. Febs Letters. 2009; 583:2593–2599. [PubMed: 19376114]

(26). Nilsson KPR, Hammarstrom P, Ahlgren F, Herland A, Schnell EA, Lindgren M, Westermark GT, Inganas O. Chembiochem. 2006; 7:1096–1104. [PubMed: 16729336]

(27). Kimura Y, Ikegami A. J. Mem. Biol. 1985; 85:225–231.

(28). Nile Red has previously been reported to emit fluorescence at different wavelengths upon binding to different amyloid fibrils in solution. Nile Red was not, however, capable of discriminating Aβ versus prion fibrils. Additionally, Nile Red is not suitable for histological studies due to its poor selectivity for binding to amyloid plaques compared to other biologics present in tissue. See ref 22.

(29). Mataga N, Kaifu Y, Koizumi M. Bull. Chem. Soc. Jpn. 1955; 28:690–691.

(30). Bagchi B, Oxtoby DW, Fleming GR. Chem. Phys. 1984; 86:257–267.

(31). Lakowicz, JR. Principles of fluorescence spectroscopy. Kluver Academic/Plenum; New York: 1999.

(32). The linear relationship between Stokes shifts of **1-3** and their observed λ_{max} for fluorescence emission was essential to estimate ε_0 for the binding pocket of the amyloids since the background absorption of tissue and limitations in the laser source for excitation of fluorophores in the confocal microscope would not allow for measurement of the Stokes shift of **1-3** in the tissue samples.

(33). This property is relatively common for many fluorophores. See ref. 31.

(34). Haynes, WM., editor. CRC Handbook of Chemistry and Physics. 92nd Edition ed. CRC Press/ Taylor and Francis; Boca Raton, FL: 2012. Permittivity (Dielectric Constants) of Liquids.

(35). Here, we assume that extremely acidic environments of pH < 1.7 within the binding pocket of amyloid deposits is unlikely.

(36). Cordeiro MF, Guo L, Coxon KM, Duggan J, Nizari S, Normando EM, Sensi SL, Sillito AM, Fitzke FW, Salt TE, Moss SE. Cell Death Dis. 2010; 1:e3. [PubMed: 21364622]

(37). Koronyo-Hamaoui M, Koronyo Y, Ljubimov AV, Miller CA, Ko MK, Black KL, Schwartz M, Farkas DL. Neuroimage. 54:S204–S217. [PubMed: 20550967]

(38). Ning A, Cui JZ, To E, Ashe K. Hsiao, Matsubara JA. Invest. Opthalmol. Vis. Sci. 2008; 49:5136–5143.

(39). Shimazawa M, Inokuchi Y, Okuno T, Nakajima Y, Sakaguchi G, Kato A, Oku H, Sugiyama T, Kudo T, Ikeda T, Takeda M, Hara H. J. Neurochem. 2008; 107:279–290. [PubMed: 18691390]

(40). Guo L, Duggan J, Cordeiro MF. Curr. Alzheimer Res. 2010; 7:3–14. [PubMed: 20205667]

(41). Guo L, Salt TE, Luong V, Wood N, Cheung W, Maass A, Ferrari G, Russo-Marie F, Sillito AM, Cheetham ME, Moss SE, Fitzke FW, Cordeiro MF. Proc. Natl. Acad. Sci. USA. 2007; 104:13444–13449. [PubMed: 17684098]

(42). Goldstein LE, Muffat JA, Cherny RA, Moir RD, Ericsson MH, Huang X, Mavros C, Coccia JA, Faget KY, Fitch KA, Masters CL, Tanzi RE, Chylack LT, Bush AI. Lancet. 2003; 361:1258–1265. [PubMed: 12699953]

(43). Moncaster JA, Pineda R, Moir RD, Lu S, Burton MA, Ghosh JG, Ericsson M, Soscia SJ, Mocofanescu A, Folkerth RD, Robb RM, Kuszak JR, Clark JI, Tanzi RE, Hunter DG, Goldstein LE. PLoS One. 2010; 5:e10659. [PubMed: 20502642]

(44). Feany MB, Dickson DW. Ann. Neurol. 1996; 40:139–148. [PubMed: 8773594]

(45). Skovronsky DM, Lee VM-Y, Trojanowski JQ. Annu. Rev. Pathol. Mech. Dis. 2006; 1:151–70.

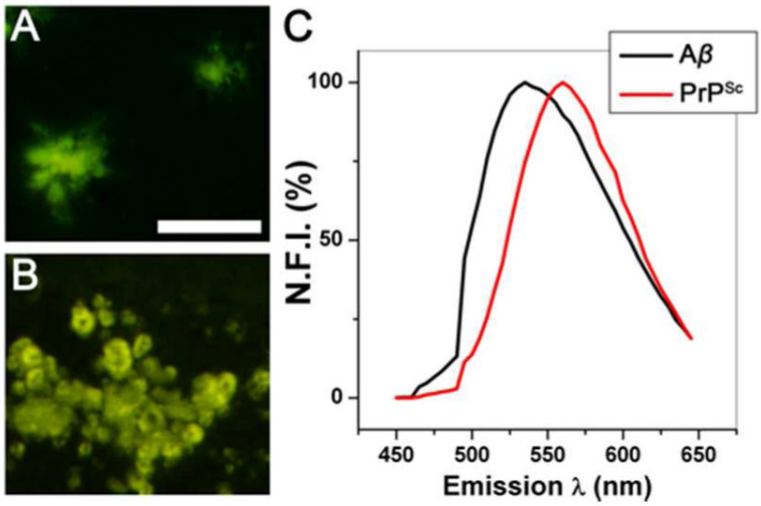

Figure 1.

True color imaging of amyloid deposits in tissue stained with ANCA probe **1**. (A) Aβ deposits in the hippocampus of an AD mouse model. (B) PrP^{Sc} deposits in the corpus callosum of a prion-infected mouse. (C) *Ex vivo* fluorescence spectra of stained deposits showing distinct emission maxima for Aβ and PrP^{Sc}. Scale bar = 100 Bm. N.F.I. = Normalized Fluorescence Intensity.

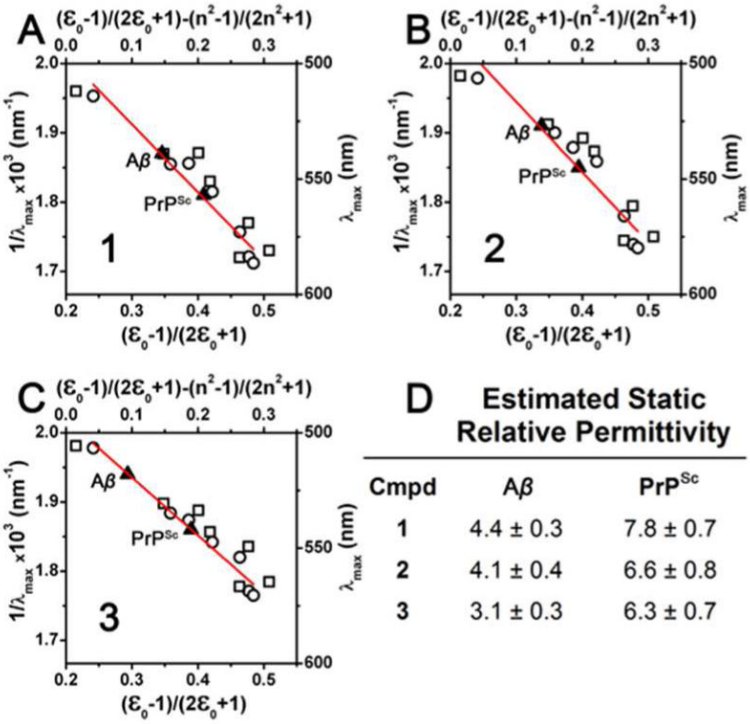

Figure 2.

Dependence of fluorescence emission of probes **1-3** on the polarity of different organic solvents. (A-C) Graphs of the relationship between $1/\lambda_{max}$ for emission of **1-3** as functions of solvent static relative permittivity (ε_0), with (open squares, □) or without (open circles, ○) the contribution of refractive index (*n*). For each graph, the linear fits of the data according to eq. 2 are shown in red, excluding the contribution from *n*. (D) Estimated ε_0 for the binding pockets of A*β* and PrP^{Sc} deposits extrapolated from the observed λ_{max} for emission of **1-3** in tissue samples.

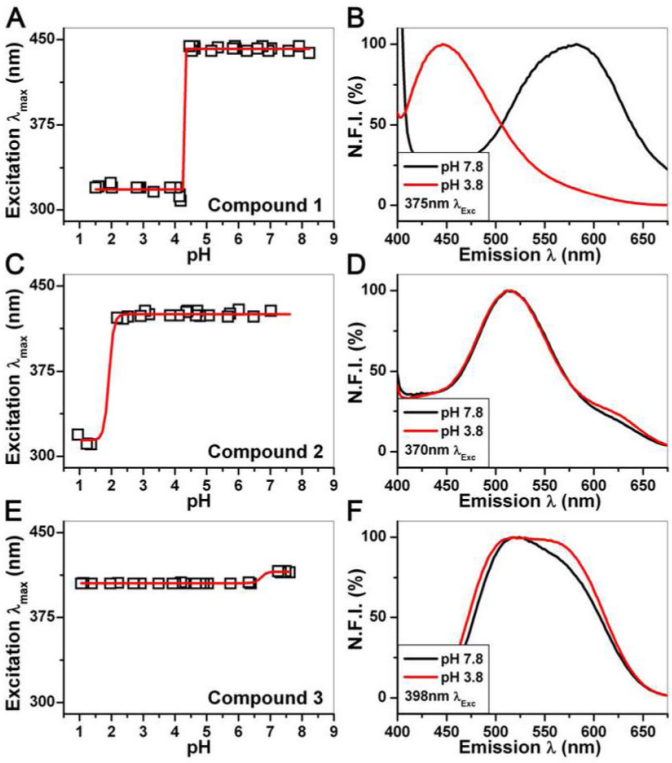

Figure 3.

Plots of absorption (A, C, E) and emission (B, D, F) λ_{max} versus pH of probes **1-3**. For fluorescence emission spectra, we chose an excitation λ_{max} that was maximized at pH 3.8 and 7.8.

Table 1

Structure, binding, and emission properties for ANCA probes **1-3** bound to amyloid proteins (see Figures S2 and S3 in the SI for additional details).

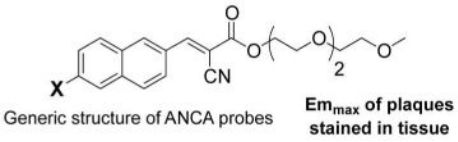

Generic structure of ANCA probes

Em_{max} of plaques stained in tissue

cmpd	X	K_d for binding to Aβ fibrils(μM)	A β (nm)	PrP^{SC} (nm)
1		1.4±0.2	535±3	554±2
2		13.8±3.1	525±4	541±4
3		4.6±1.3	515±4	538±3